https://doi.org/10.5194/egusphere-2025-1279
Preprint. Discussion started: 26 March 2025

Satellite impact of Carrington-level geomagnetic storm particle fluxes and fluences

Anton Fetzer[1], Mikko Savola[2], Adnane Osmane[2], Vili-Arttu Ketola[2], Philipp Oleynik[3], and Minna Palmroth[2,4]

[1]School of Electrical Engineering, Aalto University, Maarintie 8, 02150 Espoo, Finland
[2]Department of Physics, University of Helsinki, Helsinki, Finland
[3]Department of Physics, University of Turku, Turku, Finland
[4]Space and Earth Observation Centre, Finnish Meteorological Institute, Helsinki, Finland

Correspondence: Anton Fetzer (Anton.Fetzer@aalto.fi)

Abstract. The estimated recurrence rates of the most extreme space weather events, like the Carrington event of 1859, warrant investigations of their potential impact on modern satellite-based infrastructure. Our study is based on Extreme Value Theory (EVT) and radial diffusion to estimate worst-case particle fluxes and fluences of relativistic radiation belt (RB) electrons and solar energetic particles (SEPs) for a Carrington-level geomagnetic storm. We use Geant4 to assess the Total Ionizing Dose (TID), Single Event Upset (SEU) rates, and solar cell degradation as a result of such conditions. We find that the electron and proton fluxes exceed the fluxes experienced by the Van Allen probes during nominal conditions by more than an order of magnitude, leading up to $10\,\mathrm{krad}$ of TID behind $3\,\mathrm{mm}$ of aluminium equivalent shielding. This is equivalent to ten years of nominal operation on geosynchronous orbit and exceeds a century of nominal exposure on the orbit of the International Space Station. Our results show that the expected SEU rates in radiation-hardened satellite electronics would remain below one SEU per MByte per day, equivalent to the nominal rate received in the Van Allen belts. Satellites on lower orbits would experience an increase in SEU rates by up to four orders of magnitude compared to nominal conditions. For satellites using non-radiation hardened, off-the-shelf electronics, this would mean potentially disruptive SEU rates. We estimate up to $3\,\%$ reduction in solar cell power output assuming typical cover glass thicknesses, potentially shortening operational lifetimes or requiring mission adjustments. In conclusion, conservatively designed satellites using adequate shielding and radiation-hardened components would likely survive the outlined scenario, experiencing only accelerated ageing during the event. Satellites lacking adequate shielding or radiation-hardening would be disproportionately affected, emphasizing the importance of incorporating radiation resilience into future satellite designs and mission planning.

1 Introduction

The Carrington event of 1859 was the most extreme directly observed space weather event of modern times (Townsend et al., 2003; Rodger et al., 2008). It became famous due to its exceptional auroral displays, visible even in the Caribbean (Hayakawa et al., 2019), and disruption of telegraph lines on the ground (Boteler, 2006). No comparable superstorms have occurred during the satellite era, while the annual recurrence rate has been estimated to be $0.7\,\%$ (Chapman et al., 2020), translating to

https://doi.org/10.5194/egusphere-2025-1279
Preprint. Discussion started: 26 March 2025

roughly once per 143 years. As society increasingly relies on satellites and space-based services (Olla, 2009), a repeat event of comparable scale would be far more disruptive than in 1859. Odenwald et al. (2006) estimated that an extreme once-in-100-year space weather event could lead to the loss of $9\,\%$ of the then-operating satellite fleet. Given our growing orbital infrastructure and the recurrence rate of the most extreme superstorms, it is critical to understand the potential satellite impact of extreme solar and geomagnetic phenomena.

Space weather is a general term for the "conditions on the Sun and in the solar wind, magnetosphere, ionosphere and thermosphere that can influence the performance and reliability of space-borne and ground-based technological systems" (Doherty et al., 2004). Space weather is driven by both solar eruptions (Schwenn et al., 2005) and the dynamics of the Earth's magnetosphere, especially its radiation belts (RBs), which are torus-shaped regions with magnetically trapped high-energy particles (Koskinen and Kilpua, 2022). Observations with NASA's Van Allen Probes (Reeves et al., 2011; Horne et al., 2005) show that the radiation belts are highly dynamic, with various competing particle transport, acceleration, and loss mechanisms that are due to kinetic-scale fluctuations violating the first adiabatic invariant and large-scale fluctuations violating the second and third adiabatic invariants (see, e.g., Osmane et al. (2023) and references therein).

Space weather impacts on space-based infrastructure include temporary or permanent failure of satellites (Valtonen, 2005). The main impact on satellite technology in Earth's radiation environment is due to: 1) relativistic RB electrons accelerated by magnetospheric processes (Friedel et al., 2002), and 2) solar energetic protons (SEPs) accelerated by solar and solar wind drivers (Vainio et al., 2009). The relativistic RB electron population is maintained for long durations, posing a long-term threat to satellites (Glauert et al., 2018). SEP fluxes on satellite orbits are short-lived compared to the relativistic trapped electrons and their effects predominantly last for the duration of the SEP event (Spjeldvik, 2000). SEPs are mostly protons, some of which have such high energy that they can penetrate satellite shielding or even entire satellites (Malandraki and Crosby, 2018).

Hands et al. (2018) used modelling and statistical investigations to determine that the main effects on satellites by trapped RB electrons are the cumulative total ionising dose (TID) and displacement damage (DD). The primary impact of SEP events, as presented by Jiggens et al. (2019), are single event upsets (SEUs) and single event latch-ups (SELs) which disrupt satellite control and data handling systems. Another problem is the ageing of solar panels. Hands et al. (2018) estimated an approximately $7.6\,\%$ drop in solar cell power output on geostationary orbit after a once in 150-year solar storm caused mainly by trapped RB electrons. Horne et al. (2018) carried out an extrapolation to a realistic worst-case once in 150-year fast solar wind scenario and found that $2.5\,\mathrm{mm}$ of aluminium are required to protect satellites against internal charging due to relativistic RB electrons.

Modern satellite hardware relies on semiconductor devices for all mission-critical functions. A change of properties due to microscopic influence caused by charged particles may lead to malfunction, which can be intermittent or permanent (Rathod et al., 2011; Hughes and Benedetto, 2003). Permanent changes are caused by absorbed energy, or radiation dose, which gradually ages the semiconductor devices and changes their electrical properties. A Carrington-like storm can introduce rapid and irreversible ageing, leading to loss of mission or reduced mission lifetime after the storm. SEL may be fatal for a microchip as it opens a low-ohmic channel between the supply voltage and the supply return, which destroys semiconductor devices by overheating. SEU may corrupt memory contents (Bagatin et al., 2017), such as operating software or decision-critical data,

https://doi.org/10.5194/egusphere-2025-1279
Preprint. Discussion started: 26 March 2025

leading to loss of control or communication with the spacecraft (Binder et al., 1975; Brautigam, 2002). However, with proper design efforts, both SEL and SEU can often be mitigated (Normand, 1996; Chatzikyriakou et al., 2018). The first step towards mitigation is to estimate the rate of these errors, which could far exceed conventional design limits in a Carrington-like storm yet to be seen in the space era.

This paper presents part of the Research Council of Finland Carrington project results, which assessed the impact of a once-in-100-year space weather event on Finland's critical infrastructure. Here, we focus on satellite-based infrastructure, examining how both relativistic radiation belt (RB) electrons and solar energetic protons (SEPs) affect satellites ranging from those following ESA/NASA standards to more recent "new-space" platforms using off-the-shelf components and minimal requirements. We extrapolate worst-case fluxes of relativistic RB electrons in low-Earth orbit (LEO) by combining Extreme Value Theory (EVT) and a radial diffusion model Brautigam and Albert (2000), whereas we only use EVT to obtain extreme solar proton spectra. We then perform GEANT-4 simulations (Agostinelli et al., 2003; Allison et al., 2006, 2016) to estimate the resulting total ionizing dose, single-event effects, and potential solar cell degradation. In addition, we assess how these impacts scale with shielding and design choices across the currently operational satellite fleet. Finally, we discuss the broader implications for satellite mission lifetimes and reliability under Carrington-scale conditions. The paper is organised as follows: The EVT analysis to obtain the flux estimates is described in Sect. 2 of this paper. Sect. 3 details the GEANT-4 simulations used to estimate total ionizing dose, single-event effects, and solar cell degradation. Sect. 4 discusses the results and concludes with an overview of the potential consequences for Finland's access to space-based services in case of a repeat of the Carrington event.

2 Assessing fluxes

2.1 Extreme value theory (EVT)

In this report, we estimate the magnitude of electron fluxes using the purely statistical approach offered by EVT. EVT is a branch of statistics for estimating the tail distribution of observationally measured quantities that are rare or difficult to obtain otherwise. EVT has been successfully used to estimate the occurrence rate of rare events in a wide range of disciplines, e.g. in finance to quantify crashes (Embrechts et al., 1997), in space physics to estimate extreme solar flares (Elvidge and Angling, 2017) and in epidemiology and social sciences to estimate the potential impact of pandemics or wars on the global population (Cirillo and Taleb, 2020) and (Cirillo and Taleb, 2016). In the present case, we are interested in the maximum electron fluxes that can arise under strong geomagnetic driving conditions. For this purpose, EVT provides a rigorous statistical approach to a multiscale physics problem that is highly complex from both a computational and physics perspective (Osmane et al., 2023).

Let $X_1, \ldots, X_N$ be i.i.d. random variables with a common Cumulative Distribution Function (CDF) $F(X)$ that belongs to the Maximum Domain of Attraction (MDA) of the General Extreme Value (GEV) distribution. The GEV distribution is a family of continuous probability distributions used to model the largest (or smallest) values in a dataset. It combines three types of extreme value distributions (Gumbel, Fréchet, and Weibull) into a single framework, making it highly versatile for applications in many quantitative fields (Embrechts et al., 1997).

https://doi.org/10.5194/egusphere-2025-1279
Preprint. Discussion started: 26 March 2025

The required assumptions for EVT are: 1) i.i.d. samples coming from a common continuous distribution and 2) stationarity of the process (Pickands, 1975). If the assumptions are satisfied, the Pickands–Balkema–de Haan theorem (PBdH) of EVT states that for a random variable X, the asymptotic tail distribution above a threshold u, that is, $P(Y = X - u|X > u)$, is equal to the generalised Pareto distribution:

$$GPD_{\xi,\sigma}(y) = \tag{1}$$

$$H(y) = \begin{cases} 1 - (1 + \frac{\xi y}{\sigma})^{-\frac{1}{\xi}} & , \xi \neq 0 \\ 1 - e^{-\frac{y}{\sigma}} & , \xi = 0 \end{cases} \tag{2}$$

where ξ is the shape parameter and $\sigma > 0$ is the scale parameter. In Equation 1, $y \geq 0$ when $\xi \geq 0$ and $0 \leq y \leq \frac{-\sigma}{\xi}$ when $\xi < 0$ (Embrechts et al., 1997) (Coles, 2001). The idea is to fit a GPD to the data to obtain estimates $\hat{\xi}$ and $\hat{\sigma}$ and then use those values to determine the recurrence level, which represents the expected magnitude of the flux for an event occurring once every arbitrary number of years.

An initial estimate for ξ can be obtained using Hill's and Pickand's estimators

$$\hat{\xi}^H_{k,n} = \frac{1}{k}\sum_{i=1}^{k} \ln(X_{i,n}) - \ln(X_{k,n}), \;\; 2 \leq k \leq n \tag{3}$$

and

$$\hat{\xi}^P_{k,n} = \frac{1}{\ln 2} \ln \frac{X_{k,n} - X_{2k,n}}{X_{2k,n} - X_{4k,n}}, \;\; 1 \leq k \leq \frac{n}{4} \tag{4}$$

respectively, where $X_{k,n}$ is the upper kth upper order statistic from a sample size of n. Plotting both estimators as functions of k, often reveals a section at the beginning of the graph where the estimator is relatively constant. The value of this plateau can then be used as a rough estimate for ξ. If $\xi > -0.5$, a maximum likelihood estimate (MLE) provides a more accurate value. Note that the Hill estimator is only valid for $\xi > 0$, whereas the Pickands estimator introduces a trade-off between bias and variance. For small k, the variance is larger, while for large k, the estimator's bias increases.

2.1.1 Peaks-over-threshold (POT)

When studying small datasets of rare events, discarding too many data points can compromise the effectiveness of the EVT analysis. One approach for small datasets is the peaks-over-threshold (POT) method, which models exceedances above a threshold u by retaining all data points above u (Coles, 2001). As stated before, the assumption about i.i.d. random variables must hold, which requires declustering the data. When modelling, for example, geomagnetic activity with statistically dependent storms, only a single data point over several days can be used to ensure independence. The declustering is done by identifying local maxima $> u$ and then calculating the autocorrelation of the obtained sample with a time lag of one step. If the autocorrelation is small, the data points are assumed to be approximately independent (Coles, 2001).

We use a declustering parameter τ to enforce independence in our flux data, requiring that each local maximum be separated by at least τ time steps. We also set a threshold value $u = u_0$ for POT and try different values of u_0 and τ to see when the

https://doi.org/10.5194/egusphere-2025-1279
Preprint. Discussion started: 26 March 2025

parameter estimates become stable within calculated confidence intervals of one standard deviation. Above some $u = u_0$, the shape parameter should be constant while the scale parameter is a function of u.

2.1.2 Threshold selection

Applying EVT requires first identifying a reasonable threshold value u. Four different tools can be used for this purpose: the quantile-quantile plot (QQ), mean-excess plots, maximum-to-sum plots and Zipf plots (Embrechts et al., 1997). The main goal of using these is to see whether the data comes from a fat-tailed distribution and from which point on the Paretian behaviour kicks in since that point is a reasonable first guess for u_0.

2.1.3 Model validation

The values of $\hat{\xi}$ and $\hat{\sigma}$ can be validated using QQ plots and probability plots. In a probability plot, the pairs are plotted as (Coles, 2001)

$$\left\{ \left(\frac{i}{n_u + 1}, \hat{H}(y_i) \right) ;\ i = 1, ..., n_u \right\} \tag{5}$$

where $\hat{H}$ is the GPD evaluated using the estimates $\hat{\xi}$ and $\hat{\sigma}$ and $y_1 \leq y_2 \leq ... \leq y_{n_u}$ are the excesses above u. The pairs constitute the empirical probabilities and the probabilities from the GPD using the estimated parameter values. In a QQ plot, the sample quantiles are plotted against the corresponding model quantiles by inverting $\hat{H}$ which involves plotting the following pairs (Coles, 2001)

$$\left\{ \left(\hat{H}^{-1} \left(\frac{i}{n_u + 1} \right), y_i) \right) ;\ i = 1, ..., n_u \right\} \tag{6}$$

where $\hat{H}^{-1}(y) = u + \frac{\hat{\sigma}_H}{\hat{\xi}} \left(y^{-\hat{\xi}} - 1 \right)$. In Equation 5, the denominator $n_u + 1$ in the empirical distribution is used to avoid the empirical distribution becoming 1 for any i. If the probability and QQ plots are straight lines with slopes close to or equal to 1 and a high R^2 value, that indicates high model validity for the used data. This is a minimal requirement for using the model to extrapolate further into the tail.

2.1.4 Recurrence levels

Once the parameters $\hat{\xi}$ and $\hat{\sigma}$ are quantified, the estimate $\hat{x}_m$ for the m-year recurrence values can be computed, i.e. how large an event can be expected to take place once during a period of m years (Coles, 2001).

$$\hat{x}_m = u + \frac{\hat{\sigma}}{\hat{\xi}} \left[(n_h m \frac{n_u}{N})^{\xi} - 1 \right] \tag{7}$$

where n_h is the number of hours in a year (Since our sample resolution is one hour; for daily measurements, n_h is equal to the number of days in a year) and $\frac{n_u}{N}$ is the observed probability of an event to be larger than u. We calculate the error of the recurrence levels using the delta method from Coles (2001).

https://doi.org/10.5194/egusphere-2025-1279
Preprint. Discussion started: 26 March 2025

2.2 Relativistic radiation belt electrons

The electron data consists of differential electron fluxes for 130 keV, hereafter referred to as Fe_{130}. It was calculated by Borowsky and Yakymenko (2017), based on data from the SOPA instrument (Cayton and Belian, 2007) that consisted of instruments on multiple space crafts on geosynchronous orbit. The electron fluxes have been derived as follows. Each satellite measures the electron flux at $10\,\mathrm{s}$ intervals. From these values, 6-minute median values are calculated for each satellite, and from these median values within one hour, an hourly maximum from all the satellites is picked as the measurement value for the given hour.

The fluxes of geomagnetic storms, contained in Fe_{130}, were identified using the same identification criteria as in Simms et al. (2014). In the current analysis, we used values $k = 19$ and $n = 40$ to specify the length of the subsample within which a Dst minimum was searched for. $Dst_{onset} = -30\,\mathrm{nT}$, $Dst_{rec} = -30\,\mathrm{nT}$ and $T = 10$ were used to delimit a storm temporally. In total 316 storms were identified. Of these, we chose for further analysis only those that consisted of uninterrupted measurements, i.e. those without missing or corrupted values.

The focus on enhanced magnetospheric energetic electrons, rather than magnetospheric energetic protons, is not fortuitous. The most energetic electrons are accelerated locally within the radiation belts. Since the radiation belts confine particles, the magnetically trapped energetic electrons have a higher density than those arriving from outside the magnetosphere. Trapped protons are not energized locally as efficiently as the trapped electrons. One finds trapped protons in the inner belts but they are understood to have less variability (and thus less dependence) on a Carrington-style event. For these reasons, we focus only on relativistic RB electrons and SEPs, neglecting solar electrons or RB protons.

2.2.1 Electron peak flux spectrum estimate

Using EVT, we compute the maximum electron fluxes for a one in a hundred years event. The details of the EVT analysis to extract the fluxes of 130 keV and 1.2 MeV electrons at geosynchronous orbit can be found in (Savola, M. et al., 2025). Once we obtain the maximum fluxes, we assume an energy power-law for the fluxes. The result is the following particle distribution function:

$$f = f_0 \left(\frac{E}{E_0} \right)^{-\alpha}, \tag{8}$$

with the parameters

$f_0 = 10^{10}\,\mathrm{cm}^{-2}\,\mathrm{s}^{-1}\,\mathrm{sr}^{-1}$,
$E_0 = 0.13\,\mathrm{MeV}$, and
$\alpha = 3.7$.

The spectrum is assumed to be omnidirectional isotropic for estimating the satellite impact. The assumption of isotropic particle fluxes is justified as local anisotropies in particle flux average out across the wide range of considered orbits and

https://doi.org/10.5194/egusphere-2025-1279
Preprint. Discussion started: 26 March 2025

spacecraft attitude modes. Given the limited data on flux anisotropies during extreme events, this approach simplifies modelling and is practical. Integrating the isotropic spectrum over the full solid angle produces a factor of 4π and removes the unit sr^{-1}. Therefore,

$$f_0 = 4\pi \cdot 10^{10}\,\mathrm{cm}^{-2}\,\mathrm{s}^{-1}. \tag{9}$$

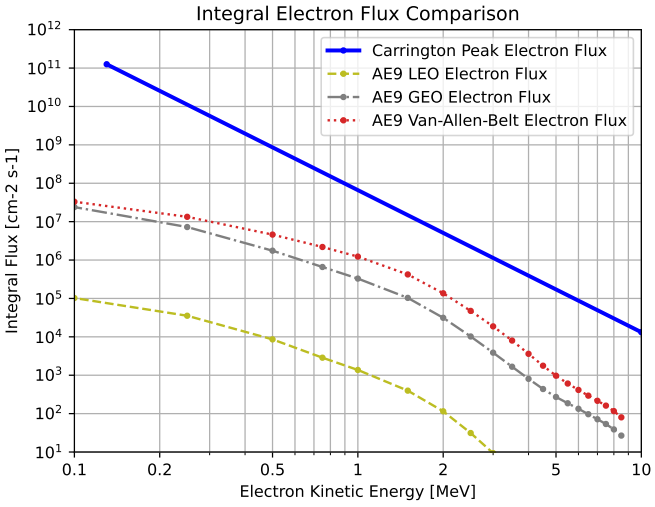

Figure 1. Comparison of the estimated peak integral Carrington electron flux with flux spectra predicted by the AE9 model for three different orbits and nominal conditions. The models and parameters used to obtain the reference spectra are shown in Tables 1 and 2. The Carrington peak electron flux is at least one order of magnitude higher than the average electron flux predicted by AP9 for the orbit of the Van Allen Belt probes and geostationary orbit and exceeds the expected electron flux on the LEO of the ISS by more than four orders of magnitude.

Figure 1 compares the peak electron flux presented in Equations 8 with mission average electron fluxes predicted by the AE9 model for nominal conditions of three different orbits. To generate these reference spectra, ESA's SPace ENVironment Information System (SPENVIS) was used Donder et al. (2018); Heynderickx et al. (2000, 2004, 2005); Kruglanski et al. (2009). It allows the user to retrieve particle spectra along spacecraft trajectories specified through a convenient web-user interface. The orbit parameters used to generate the reference spectra are presented in Table 1, while the model parameters are shown in Table 2.

https://doi.org/10.5194/egusphere-2025-1279
Preprint. Discussion started: 26 March 2025

Table 1. Parameters used to generate the trajectories in SPENVIS along which the particle fluxes for nominal conditions were calculated that were used as references throughout this publication. The generated trajectories do not account for solar radiation pressure or atmospheric drag. The Low Earth Orbit (LEO) corresponds to the altitude and inclination of the ISS. Similarly, the perigee, apogee and inclination of the Van-Allen Belt probes were used to construct a realistic worst-case reference for nominal conditions in Earth orbit.

Parameter	LEO	GEO	Van-Allen Belt Probes
Orbit type	general	geostationary	general
Orbit start	01. Jan. 2025 00:00:00	01. Jan. 2025 00:00:00	01. Jan. 2025 00:00:00
Trajectory duration	30 days	30 days	30 days
Longitude	-	0°	-
Perigee altitude	400 km	-	618 km
Apogee altitude	400 km	-	30 414 km
Inclination	51.6°	-	10.2°
Right Ascension of Ascending Node	0°	-	0°
Argument of perigee	0°	-	0°
True anomaly	0°	-	0°

https://doi.org/10.5194/egusphere-2025-1279
Preprint. Discussion started: 26 March 2025

Table 2. Particle model parameters used in SPENVIS to estimate the particle fluxes for nominal conditions used as reference throughout this publication. The AE9/AP9 models Ginet et al. (2013) estimate trapped electron and proton fluxes in the radiation belts. The SAPPHIRE model Jiggens et al. (2018) estimates long-term average solar proton and heavy ion fluxes. The ISO-15390 model International Organization for Standardization (2018) provides cosmic ray proton and heavy ion fluxes, while the CREME-96 model Tylka et al. (1997) provides the worst 5-minute flux observed in October 1989 by the GOES satellite.

Parameter	Value
Model	AE9/AP9
Model version	1.5
Model run mode	mean
Model	SAPPHIRE (total fluence)
Prediction Period	automatic
Offset in solar cycle	automatic
Confidence level	50 %
Magnetic shielding	default
Model	ISO-15390 standard model
Solar activity data	mission epoch
Magnetic shielding	default
Model	CREME-96
Mode	Peak 5-minute-averaged fluxes
Magnetic shielding	default

2.2.2 Electron flux time dependence and event fluence

To estimate the lifetime of fluxes, we use the empirically dependent radial diffusion model of Brautigam and Albert (2000) for a geomagnetic Kp index equal to 8, and with the parameters estimated by Sarma et al. (2020). The time-dependent particle flux
190 $f(t)$ during a Kp=8 event would follow an exponential decay, as in

$$f(t) = f_0 \cdot \exp\left\{\frac{-t}{T_c}\right\} \tag{10}$$

with the flux amplitude f_0 as in equation 9, the time t and the decay constant $T_c = 1.23\,\mathrm{d}$ Sarma et al. (2020).

The fluence F is the time integral of the flux.

https://doi.org/10.5194/egusphere-2025-1279
Preprint. Discussion started: 26 March 2025

$$F = \int_0^T f_0 \cdot \exp\left\{\frac{-t}{T_c}\right\} \mathrm{d}t \tag{11}$$

$$= f_0 \left(T_c - T_c \exp\left\{\frac{-T}{T_c}\right\}\right) \tag{12}$$

For $\lim_{T\to+\infty}$ the exponential term approaches zero, from which follows

$$\lim_{T\to+\infty} F(T) = f_0 \cdot T_c = f_0 \cdot 1.23\,\mathrm{d} = f_0 \cdot 29.52\,\mathrm{h} = 1.335 \times 10^{16}\,\mathrm{cm}^{-2} \tag{13}$$

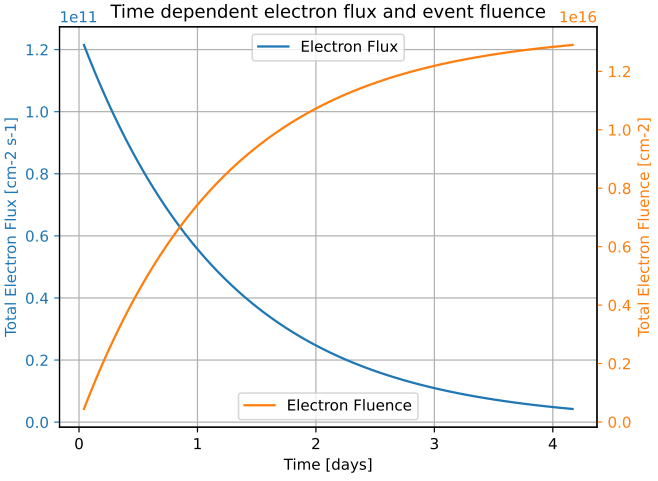

Figure 2. Time-dependent relativistic RB electron flux and accumulated event fluence for a Kp=8 event according to Equation 10. Approximately half of the event fluence is received in the first 24 hours.

2.3 Solar energetic protons

2.3.1 Solar proton flux spectrum estimate

For solar energetic protons, we use the annual integral solar proton fluences for 1984-2019 (Raukunen, O. et al., 2022) and apply once more an EVT analysis with maximum fluxes over 150 years estimated separately for 10 MeV, 30 MeV, 60 MeV, 100 MeV and 200 MeV. The results are shown in Table 3.

https://doi.org/10.5194/egusphere-2025-1279
Preprint. Discussion started: 26 March 2025

Table 3. Solar proton fluxes estimated from the extreme value analysis methodology described in Sect. 2.1 and with the data of Raukunen, O. et al. (2022).

	Solar proton flux [$\mathrm{cm^{-2}\,s^{-1}\,sr^{-1}}$]		
Energy [MeV]	-2 Sigma	Expected	+2 Sigma
10	22 000	46 000	130 000
30	5600	8500	16 000
60	1400	2300	5400
100	430	1100	4400
200	110	290	1400

The Carrington solar proton spectra are assumed to be omnidirectional. The omnidirectional integral fluxes in $\mathrm{cm^{-2}\,s^{-1}}$ are used in the following.

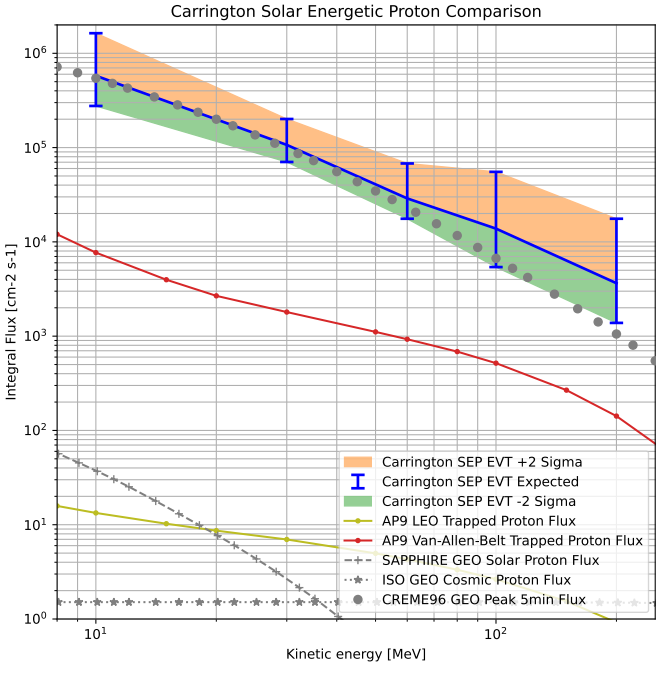

Figure 3. Comparison of the integral Carrington solar proton flux estimates with trapped proton spectra predicted by the AP9 model for the LEO of the ISS and the orbit of the Van Allen probes under nominal conditions as well as the solar proton flux predicted by the SAPPHIRE model for GEO. The models and parameters used to obtain the reference spectra are shown in Tables 1 and 2. The CREME96 peak flux averaged over 5 min observed by the GOES satellite during the October 1989 geomagnetic storm is also included (Tylka et al., 1997).

https://doi.org/10.5194/egusphere-2025-1279
Preprint. Discussion started: 26 March 2025

Figure 3 shows the estimated omnidirectional integral Carrington solar proton spectrum with ±2 sigma uncertainty bands compared to particle spectra for normal conditions in near-Earth space. The Carrington solar proton fluxes are at least one order of magnitude higher than the mission average trapped proton spectra experienced by the Van Allen probes on their orbit through the proton belts. Compared to the average trapped proton fluxes expected on the orbit of the ISS, the Carrington solar proton spectrum would correspond to an increase by four orders of magnitude. The long-term average solar proton flux on geostationary orbit is also several orders of magnitude lower. The "worst 5-minute" fluxes provided by CREME96 closely resemble the estimated Carrington event fluxes. In the Carrington case, these fluxes are expected to be sustained on the order of a couple to a few days before wave-particle interactions lead to irreversible losses Horne et al. (2005).

2.3.2 Solar proton flux time dependence and event fluence

Without a magnetospheric model that can account for magnetically trapped protons on timescales of days, the time dependence of the proton fluxes in Earth orbit during a Carrington-level space weather event remains an open question. For simplicity and as a reasonable worst-case scenario, we assume that the Carrington solar proton flux follows the same time dependence as the electron flux introduced in the previous section. This means a total event fluence equivalent to 1.23 days of sustained peak flux is assumed. For further insights into the time dependence of extreme solar proton events, we refer to the solar proton events of 1987 or 1988 and the example events provided by the NASA OLTARIS tool (Singleterry et al., 2011).

3 Satellite impact

The following estimates of the satellite impact of the extreme electron and proton fluxes are presented in Sect. 2. As introduced in Sect. 1 the three main effects on satellites during such a space weather event are component degradation due to accumulating TID, single event effects (SEE) in the satellite electronics due to particles with high linear energy transfer (LET), and degradation of satellite solar cells due to displacement dose (DD). Surface or internal charging, as well as other radiation effects, are not considered here.

Despite the large uncertainties in the flux and fluence estimates presented in the previous section, the spectra were used as if they were precise inputs for the following particle transport simulations. The presented error bars and uncertainties only account for the statistical uncertainty of the Monte-Carlo-based simulations and do not include uncertainties from the particle spectra or any other sources of uncertainty. The ±2 sigma uncertainty levels of the Carrington solar particle fluxes were simulated as separate spectra. The "+2 sigma" results shown in the following were obtained by treating the +2 sigma upper limit flux data points as a standalone particle spectrum, while the same was done for the "-2 sigma" results.

3.1 Total ionising dose

To estimate the TID received by the electronics inside satellites during a Carrington scale event, the particle fluxes of Sect. 2 were simulated against varying thicknesses of aluminium shielding. The simulation was performed with the software "Geant4 Radiation Analysis for Space" (GRAS) (Santin et al., 2005). It is based on the Geant4 Monte Carlo particle transport toolkit

https://doi.org/10.5194/egusphere-2025-1279
Preprint. Discussion started: 26 March 2025

(Allison et al., 2016, 2006; Agostinelli et al., 2003). Following the recommendation of the SPENVIS help files (ESA, 2022a), the em_standard_opt3 and QBBC physics lists were used.

A planar shielding geometry consisting of square aluminium plates on top of $0.5\,\mathrm{mm}$ thick silicon plates was used to represent the outer shielding panels of a satellite protecting the sensitive integrated semiconductor circuits inside the satellite. The particles are attenuated in the aluminium layer and deposit ionising dose in the silicon layer. This deposited dose is used to estimate the ionising dose satellite electronics would receive in such an environment. Geometry Definition Markup Language (GDML) (CERN, 2020; Chytracek et al., 2006) code was used to place 101 shielding and detector tiles next to each other such that the aluminium plates facing the particle beam form a continuous surface as shown in Figure 4. The particles are placed at random locations on the surface and enter the shielding and detector stacks with an inwards pointing cosine angular distribution representing one hemisphere of an isotropic radiation environment. The energy of the particles is sampled from the particle spectra presented in Sect. 2. The edge length of the square tiles was set to $10\,\mathrm{m}$, while the thickness of the aluminium shields is up to $10\,\mathrm{mm}$. This high width-to-depth ratio was chosen to minimise the influence of edge effects.

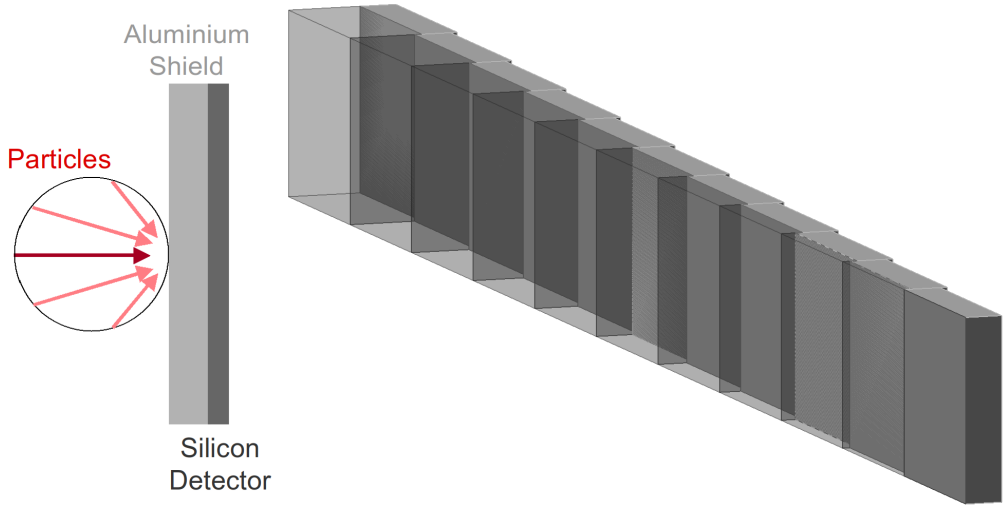

Figure 4. Sketch of a single shielding and detector tile (left) and render of the planar shielding and detector geometry (right) implemented with GDML in GRAS to determine the TID in silicon behind varying thicknesses of aluminium shielding. Each tile consists of an aluminium shield (transparent grey) and a silicon detector plate (solid grey). This visualisation only shows eleven tiles, while the simulations were performed with 101 tiles. The thickness of the plates is exaggerated to show the increase in shielding thickness between the tiles. The sketch includes the particles generated with cosine angular distribution on the surface of the aluminium shielding plate.

https://doi.org/10.5194/egusphere-2025-1279
Preprint. Discussion started: 26 March 2025

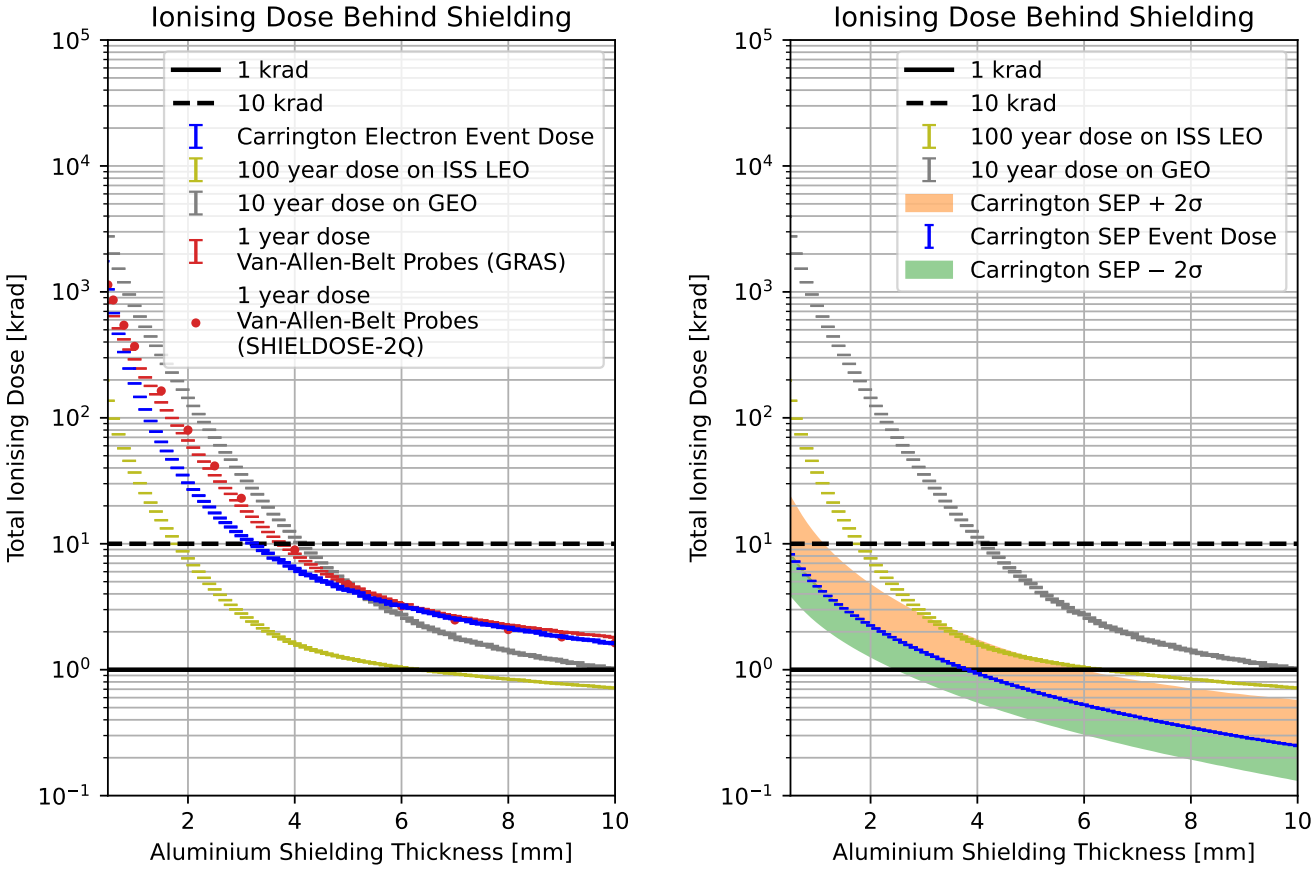

(a) TID due to Carrington relativistic RB electron event fluence.

(b) TID due to Carrington solar proton event fluence.

Figure 5. TID received in 0.5 mm silicon plates behind planar shielding of varying aluminium thickness due to the estimated Carrington RB electron event fluence (a) and solar proton event fluence (b). The dose received in 100 nominal years on the LEO of the ISS and the 10-year dose on GEO from all particle types are included for comparison. The plot on the left also includes the 1-year dose on the orbit of the Van Allen probes, which was calculated both with GRAS and SHIELDOSE-2Q to validate the simulation setup. The TID due to RB electron fluence exceeds the TID due to solar protons for all shielding thicknesses up to 1 cm of aluminium.

Figure 5 shows the resulting TID shielding curves for the Carrington solar proton event fluences, relativistic RB electron event fluence as well as total dose curves for nominal conditions on the LEO of the ISS, a GEO and the GTO orbit of the Van Allen probes. The orbit and model parameters used to estimate the nominal condition dose rates are shown in Tables 1 and 2. To validate the GRAS simulation setup, a dose curve for a geostationary transfer orbit (GTO) similar to that of the Van Allen probes was also calculated using the SHIELDOSE-2Q ionising dose for simple geometries tool on SPENVIS (Seltzer, 1980, 1994; ESA, 2018). For practical reasons, annealing and enhanced low dose rate sensitivity (ELDRS) were not considered here despite comparing dose rates that differ by orders of magnitude.

https://doi.org/10.5194/egusphere-2025-1279
Preprint. Discussion started: 26 March 2025

The main result of this comparison is that the TID received by satellites during a Carrington event is comparable to the dose satellites receive in ten nominal years on GEO and is higher than the dose received in an entire century of nominal conditions on the LEO of the ISS. If the proton and electron fluxes have the same time dependence, the dose resulting from solar protons would be lower than the dose due to trapped electrons. Even a full cm of aluminium shielding would result in more than $1\,\mathrm{krad}$ of TID due to electrons, but to exceed $10\,\mathrm{krad}$, the shielding would have to be less than $3\,\mathrm{mm}$ of aluminium equivalent.

Radiation-hard electronics can be designed to survive more than $100\,\mathrm{krad}$ (Hands et al., 2018). Only components shielded by less than $1\,\mathrm{mm}$ of aluminium would exceed this level. This suggests that satellites designed with radiation considerations in mind, such as the GPS and Galileo satellites or large geostationary communications and weather satellites, would likely survive the TID received during a Carrington event. These satellites have enough shielding to attenuate the electron flux below levels for which their radiation-hard electronics are designed. Although these satellites are expected to survive the event, their remaining operational lifespan could be reduced by several years due to premature failure caused by accumulated TID.

As mentioned in Sect. 8, applying EVT to geostationary fluxes only provides values at geostationary orbits. For the sake of simplicity, the spatial distribution of the fluxes is extrapolated using a radial diffusion model, as described in Sect. 2.1. Depending on how deep the relativistic electrons penetrate the inner magnetosphere during the event, LEO satellites could also be subjected to high fluxes of relativistic electrons. Many small satellites on LEO are not equipped with sufficient shielding or radiation-hard electronics to survive the predicted event TID due to the benign radiation environment for which they are designed. In case the predicted fluxes reach deep into the inner magnetosphere, a significant fraction of satellites could be expected to fail during the event. The satellites surviving the event would experience performance degradation due to the characteristic parameters of their semiconductor components drifting out of their designed operating range. For the satellite operators, this would appear as if the surviving satellites aged several years in only a few days. Due to this ageing, even some of the surviving satellites would have to be replaced before the end of their nominal mission duration.

3.2 Single event effects

To compare the rate of SEEs to be expected during a Carrington-level space weather event with SEE rates during nominal conditions, the spectra shown in Figure 3 were used to generate Linear Energy Transfer (LET) histograms in silicon behind different thicknesses of aluminium shielding. The LET histograms then have to be combined with the measured Single Event Upset (SEU) cross-section curve of an integrated semiconductor device representative of modern space electronics.

As in Sect. 3.1 the geometry for the particle transport simulations was defined in GDML. Due to the high computational requirements for producing the LET histograms, the different shielding thicknesses were simulated in separate runs. The geometry for each run, therefore, consisted only of one planar aluminium shielding plate on top of one silicon plate, as shown on the left side of Figure 4.

As for the TID simulations, the software GRAS was used to sample particles from the input spectra. The particles were placed on the surface of the aluminium shielding with an inward-facing cosine angular distribution to represent a hemisphere of an omnidirectional particle environment. The particles are then tracked through the shield and reach the boundary between the aluminium and silicon layers. GRAS computes the LET in silicon for each particle arriving at the boundary and tallies them

https://doi.org/10.5194/egusphere-2025-1279
Preprint. Discussion started: 26 March 2025

in LET histograms. This assumes that the sensitive transistors are at the surface of the silicon facing into the direction of the beam. The "em_standard_opt3" and QBBC physics lists were used as recommended in the SPENVIS help files (ESA, 2022a).

SEU cross-section curves and the upset rates resulting from them are strongly device-specific. This means that the upset rates estimated in this analysis are only examples that allow for relative comparison between the extreme and nominal conditions and are not meant to provide absolute estimates.

The configuration memory of the NG-MEDIUM FPGA by NanoXplore was chosen as the representative device because it is the first European-made FPGA to be awarded ESCC QPL certification (NanoXplore, 2022).

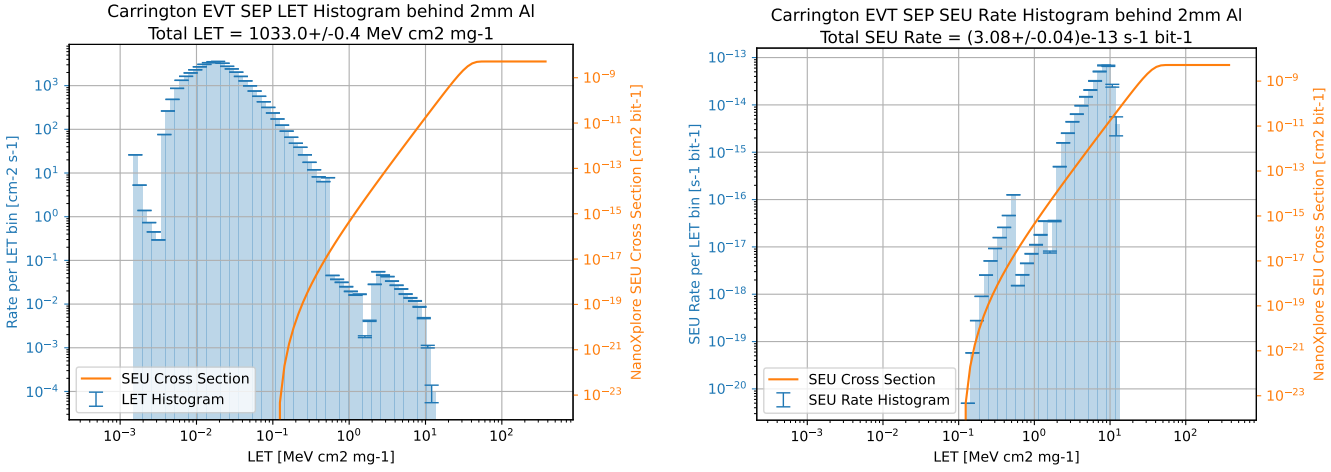

(a) LET rate histogram.

(b) SEU rate histogram.

Figure 6. Histograms of the LET rate and SEU rates due to the expected Carrington solar proton EVT spectrum in silicon behind 2 mm of planar aluminium shielding. The LET rate histogram (a) shows contributions from slowed-down protons and secondary particles, including knocked-out aluminium nuclei. The SEU rate histogram (b) was obtained by scaling the LET bins using the SEU cross-section function of the NanoXplore NG-Medium FPGA shown in Equation 14, which is also included in both of the figures. The cross-section curve parameters are shown in Table 4 and were provided by NanoXplore (2020).

An example of such a LET histogram is shown in Figure 6a. The Weibull function $f(\mathrm{LET})$ shown in Equation 14 is also included in the figure. It returns the SEU cross-section in $\mathrm{cm^2\,bit^{-1}}$ based on LET values in $\mathrm{MeV\,cm^2\,mg^{-1}}$ when using the parameters shown in Table 4 provided by NanoXplore (2020).

$$f(\mathrm{LET}) = \begin{cases} 0 & \text{if LET} \leq L_0 \\ A_0 \left(1 - \exp\left(-\left(\frac{\mathrm{LET}-L_0}{W}\right)^S\right)\right) & \text{if LET} > L_0 \end{cases} \tag{14}$$

https://doi.org/10.5194/egusphere-2025-1279
Preprint. Discussion started: 26 March 2025

L_0	W	S	A_0
$\mathrm{MeV\,cm^2\,mg^{-1}}$	$\mathrm{MeV^{-1}\,cm^{-2}\,mg}$	-	$\mathrm{cm^2\,bit^{-1}}$
0.11	36	4.4	5.2×10^{-9}

Table 4. Weibull fit parameters of the NanoXplore NG-Medium SEU cross section as provided by NanoXplore (2020). L_0 is the threshold LET value, A_0 the amplitude coefficient , W the width parameter and S the shape parameter.

To obtain an SEU rate histogram as shown in Figure 6b, each of the LET bins is multiplied with the cross-section function $f(\mathrm{LET})$ shown in Equation 14 evaluated at the mean LET of each of the LET bins. The resulting values then show the SEU rate caused by particles in the corresponding LET range. The SEU rate histogram bins are then summed to obtain the total SEU rate. This was performed for all the spectra shown in Figure 3 as well as the Carrington relativistic RB electron spectrum shown in Figure 1. Electrons can cause SEEs (Tali et al., 2019), but even the Carrington electron spectrum only resulted in negligible SEU rates, which is why electron spectra are not included in the following results. NanoXplore (2020) predict a Soft Error Rate (SER) rate of $2.05 \times 10^{-10}\,\mathrm{bit^{-1}\,d^{-1}}$ on geostationary orbit. In other units, this is equal to $2.37 \times 10^{-15}\,\mathrm{bit^{-1}\,s^{-1}}$. The value obtained with the method outlined above is between $10^{-16}\,\mathrm{bit^{-1}\,s^{-1}}$ and $10^{-15}\,\mathrm{bit^{-1}\,s^{-1}}$ depending on the shielding thickness. We consider this agreement to be sufficient to validate our method and simulation setup.

https://doi.org/10.5194/egusphere-2025-1279
Preprint. Discussion started: 26 March 2025

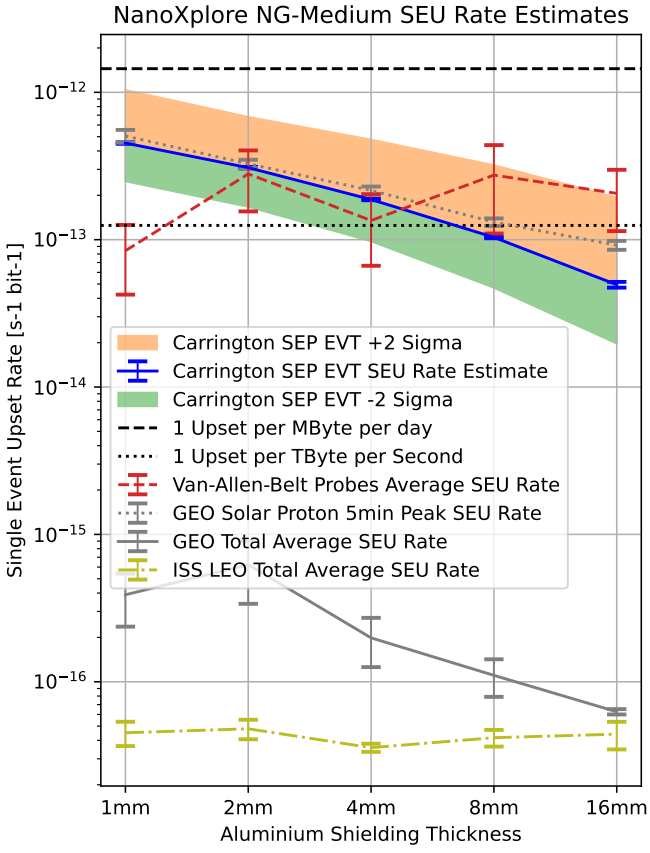

Figure 7. SEU rate estimates based on LET spectra in silicon behind planar aluminium shielding computed with GRAS combined with the SEU cross section curve in Equation 14 based on the parameters shown in Table 4 provided by NanoXplore (2020). The SEU rate due to the Carrington solar proton flux estimate depends on the shielding thickness. For the considered shielding thicknesses, the expected Carrington SEU rate is approximately the same as the SEU rate in the Van Allen belts but several orders of magnitude higher than the rates expected for nominal conditions on GEO and LEO.

Figure 7 shows the resulting SEU rates behind different thicknesses of aluminium shielding for the Carrington solar proton fluxes and nominal conditions. Increasing shielding from $2\,\mathrm{mm}$ to $16\,\mathrm{mm}$ reduces the SEU rate by an order of magnitude. The SEU rates shown for LEO, GEO and the Van Allen probe orbits (see Table 1) are the total SEU rates obtained by summing up the SEU rates due to trapped protons, solar protons, cosmic protons and cosmic iron ions based on the spectra provided by the models shown in Table 2. The nominal SEU rate on the orbit of the Van Allen probes is similar to the predicted Carrington SEU rate. The CREME96 solar proton "peak worst 5min" GEO spectrum resulted in SEU rates almost identical to the Carrington SEU rates, while the SEU rate on GEO during nominal conditions is three orders of magnitude lower. Even lower is the SEU rate for nominal conditions on LEO. If the predicted Carrington solar proton fluxes reach deep into the magnetosphere and hit lightly shielded satellites carrying integrated semiconductor devices comparable to the NanoXplore NG-Medium FPGA,

https://doi.org/10.5194/egusphere-2025-1279
Preprint. Discussion started: 26 March 2025

they would experience an increase in SEU rates by more than four orders of magnitude. Despite this dramatic increase, the SEU rate expected in this specific device would still be less than one upset per MByte per day, indicating that this proton flux would not be catastrophic for satellites designed for radiation environments. According to (NanoXplore, 2020) the NG-Medium FPGA has $6\,\mathrm{MB}$ of configuration memory. Assuming the event fluence equivalent to $1.23\,\mathrm{d}$ as introduced in Sect. 2.3.2 the NG-Medium FPGA would be expected to experience less than six SEUs during the whole event.

3.3 Solar cell degradation

The satellite solar cell power degradation during a Carrington-like event is estimated by simulating the displacement damage dose (DDD) from non-ionizing energy loss (NIEL) of the estimated proton and electron fluxes. Before the particles deposit DDD in a solar cell, they first have to pass through the cover glass. To simulate this, the MULtiLAyered Shielding SImulation Software (MULASSIS) was used, which is a Geant4-based simulation tool developed for ESA Lei et al. (2002). The Monte Carlo Solar Cell Radiation Environment Analysis Models code (MC-SCREAM) is a macro file generated by SPENVIS, which uses the DDD analysis feature of MULASSIS to calculate solar cell degradation from particle fluxes and material inputs (Messenger et al., 2008; ESA, 2022b).

The solar cell is modelled with a $10\,\mu\mathrm{m}$ gallium arsenide layer of density $5.31\,\mathrm{g\,cm^{-3}}$, with one layer of $2.32\,\mathrm{g\,cm^{-3}}$ silicon dioxide (fused quartz) cover glass. The cover glass layer thickness was varied between 20 and $800\,\mu\mathrm{m}$. The DDD deposition in the solar cell is then modelled with the "INFN/ESA 2014 21eV" NIEL dataset supplied to MULASSIS by Baur et al. (2014). According to Messenger et al. (2008), the total power degradation as a fraction of initial power ($\frac{P}{P_0}$) is semi-empirically calculated as a function of DDD (D_d) using the model parameters C and D_x from ground-based measurements as in

$$\frac{P}{P_0} = 1 - C \log\left(1 + \frac{D_d}{D_x}\right) \tag{15}$$

The Azur 3G30 solar cell is chosen because it is the default solar cell definition retrievable from SPENVIS and shows typical degradation behaviour compared to the other solar cell definitions (Ketola, 2024). The default EM Opt3 and the QBBC physics list are used. The Monte Carlo simulations are conducted with two million particles each.

As introduced in Sect. 2.2 and 2.3 it is assumed that the Carrington-scale particle fluxes are omnidirectional and that the event fluence is equivalent to 1.23 days of sustained peak flux. Additionally, the fluxes are assumed to be spatially independent due to magnetospheric compression (Tsurutani and Lakhina, 2014).

To validate the methodology, particle fluences from the Energetic Particle Sensor instrument onboard GOES-11 measured during the 2003 Halloween Storm were used to predict solar cell power degradation with MC-SCREAM. This data was retrieved from NOAA (2024). The predicted degradation is compared with the $1.4\,\%$ solar cell degradation measured by the Cluster-II spacecraft during the same space-weather event (LaBel, 2005) as shown in Figure 8a. The particle fluences for the orbits included in Figures 1 and 3 are simulated for comparison. Assuming the same fluence equivalent to 1.23 days of peak flux for both the Carrington relativistic RB electrons and the solar protons, the power degradation due to electrons is negligible in comparison with the degradation due to the proton fluxes (Ketola, 2024).

https://doi.org/10.5194/egusphere-2025-1279
Preprint. Discussion started: 26 March 2025

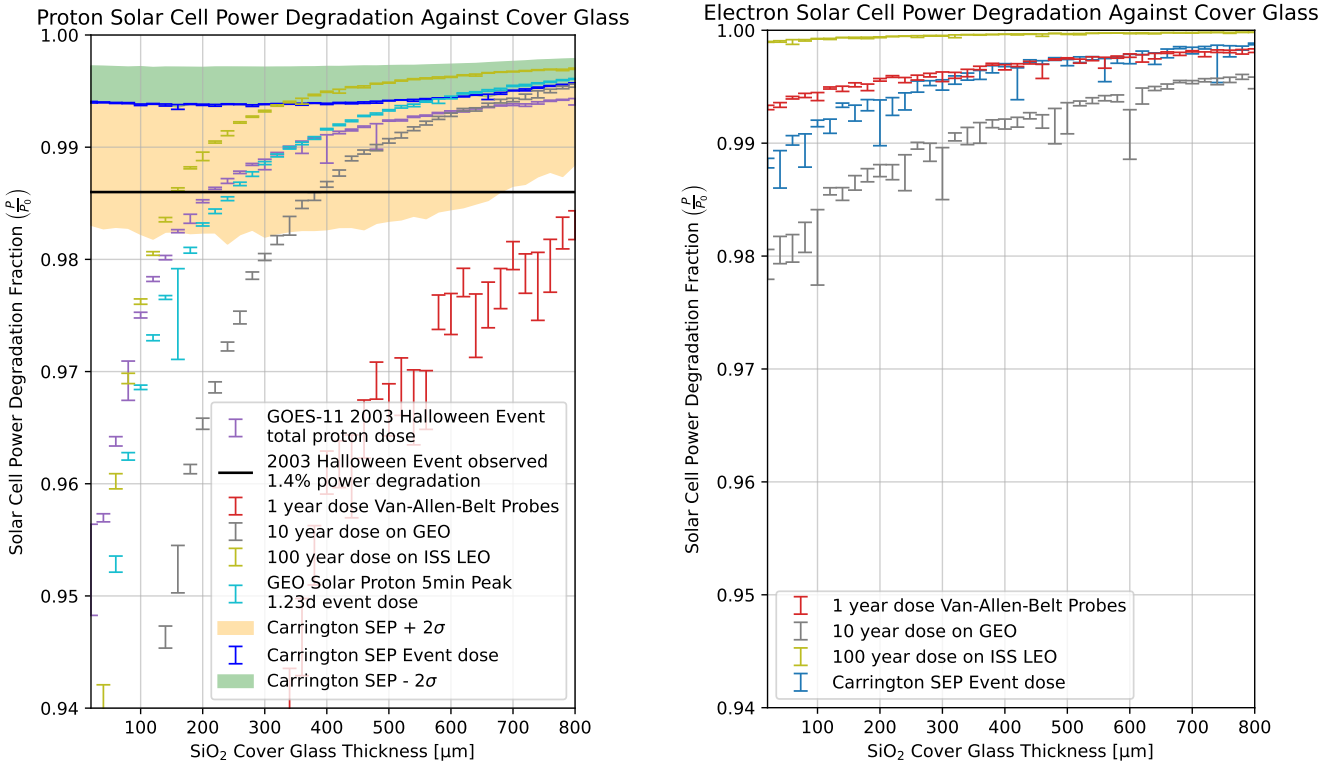

(a) Power degradation compared over proton fluences.

(b) Power degradation compared over electron fluences.

Figure 8. Power degradation as a fraction of the initial power given over the thickness of the silicon dioxide cover glass for the Azur 3G30 solar cell model retrieved from SPENVIS. Results are shown for the estimated Carrington event fluences from Sect. 2.2 and 2.3. The degradation is compared to the dose received in 100 nominal years on the LEO of the ISS, the 10-year dose on GEO, and a 1-year dose on the orbit of the Van Allen probes. In addition, the 2003 Halloween Event fluence measured by GOES-11 is used as validation against an observed $1.4\,\%$ power degradation on Cluster-II. The degradations due to proton doses are shown in (a), and the electron degradation is shown in (b).

Figure 8 shows the solar cell power degradation results as a fraction of initial power output over cover glass thickness in micrometres. The simulated degradation due to the 2003 Halloween Event fluence is near the NASA Cluster-II recorded degradation of $1.4\,\%$ for a $200\,\mu\mathrm{m}$ cover glass. Above $500\,\mu\mathrm{m}$ of cover glass thickness, all simulated fluences cause less than one percent of power degradation, with the only exception being the Van Allen probes orbit, which causes more than three percent of power degradation per year.

According to (Maurer et al., 2018) the Van Allen probes had a solar cell degradation monitor with $500\,\mu\mathrm{m}$ thick cover glass, but the degradation observed after five years was $33\,\%$, corresponding to $6.6\,\%$ per year which is almost twice as much as the $3.5\,\%$ predicted by the simulation results shown in Fig. 8.

https://doi.org/10.5194/egusphere-2025-1279
Preprint. Discussion started: 26 March 2025

The web implementation of MC-SCREAM available on SPENVIS shows a disclaimer that "data for most recent cell technologies are valid up to at least a dose of $10^{11}\,\mathrm{MeV\,g^{-1}}$ for currents and $3 \times 10^{10}\,\mathrm{MeV\,g^{-1}}$ for voltages and power" (Donder et al., 2018), which are exceeded by the simulated fluences shown in Fig. 8.

The Carrington SEP curve converges with the other scenarios only for very thick cover glasses. Unlike for nominal conditions, the degradation does not strongly depend on cover glass thickness until $500\,\mu\mathrm{m}$, which would exceed typical recommendations (NASA, 1971). The degradation due to Carrington SEPs seems to increase in severity with cover glass thickness until after approximately $200\,\mu\mathrm{m}$. This is likely due to the generation of secondary particles by very high-energy protons, as has also been found with other DDD codes (Jun, 2001).

The CREME96 GEO Peak 5 min Flux shown in Fig. 3 agrees well with the EVT estimate for the SEP flux above $10\,\mathrm{MeV}$. This agreement is also visible in Fig. 7. The strong divergence between the CREME96 GEO Peak 5 min Flux and the Carrington EVT estimate in Fig. 8 is explained by the low energy cut-off of the EVT spectrum which is at $10\,\mathrm{MeV}$, while the CREME96 spectrum extends to $0.1\,\mathrm{MeV}$. Solar cell cover glass with thicknesses below $500\,\mu\mathrm{m}$ is transparent to $5\,\mathrm{MeV}$ protons, which means the Carrington EVT flux estimate cannot be used to calculate solar cell degradation. Instead, the CREME96 GEO Peak 5 min Flux scaled to the same $1.23\,\mathrm{d}$ of peak flux equivalent fluence should be used in this case. This results in a solar cell degradation estimate for a Carrington level storm of approximately three percent for $100\,\mu\mathrm{m}$ of cover glass or only $1.5\,\%$ for satellites with $200\,\mu\mathrm{m}$ of the cover glass.

4 Discussion and conclusions

In this paper, we assessed the satellite impact of a potential Carrington scale extreme space weather event concentrating on relativistic RB electron and SEP fluxes. Since Carrington scale fluxes have not been observed during the space era, we used EVT to extrapolate from historical GEO particle flux data, producing worst-case estimates for the particle flux spectra of a Carrington-scale event. The relativistic RB electron and SEP flux estimates resulting from the EVT analysis are more than an order of magnitude higher than the electron and proton fluxes predicted for the orbit of the Van Allen probes during nominal conditions, respectively. They exceed the average proton and electron fluxes on the orbit of the ISS by more than four orders of magnitude. Our SEP flux estimate agrees with the CREME96 "worst 5-minute" fluxes between $10\,\mathrm{MeV}$ and $50\,\mathrm{MeV}$. The EVT approach with radial diffusion based on historical GEO fluxes provides an isotropic estimate regardless of orbit but gives only an approximate insight into the time dependence of the fluxes, especially in the case of proton fluxes.

Using the results from the EVT analysis, we performed Monte-Carlo particle tracking simulations with Geant4-based software to determine total ionising dose (TID) and single event upset (SEU) rates received by satellite electronics behind aluminium shielding and solar cell degradation of satellites exposed to the particle fluxes. Assuming total event fluences corresponding to 1.23 days of sustained flux, satellites are expected to receive more than $1\,\mathrm{krad}$ of TID mostly due to electrons even behind $8\,\mathrm{mm}$ of aluminium equivalent shielding. More than $10\,\mathrm{krad}$ would only be received behind less than $8\,\mathrm{mm}$ of aluminium equivalent shielding. This TID is equivalent to one year on the orbit of the Van Allen probes, ten years on GEO or more than a century on the orbit of the ISS. Our results suggest that the TID would not cause catastrophic damage to the major-

https://doi.org/10.5194/egusphere-2025-1279
Preprint. Discussion started: 26 March 2025

ity of satellites. However, it would rapidly age satellite electronics equivalent to years or even decades of operation, depending on their orbit, which could lead to the premature retirement of a significant number of satellites. The EVT approach includes uncertainty in the time dependence of the fluxes, which limits the TID estimates, as both scale linearly with the exposure time. Detailed information about orbit-specific fluxes over various timescales would be required to predict the impact on different satellites, especially on LEO, more precisely.

Our results show less than one SEU per MByte per day in shielded radiation-hardened electronics, which also suggests that conservatively designed satellites would likely survive such an event. If an important part of the software of a satellite onboard computer is corrupted, the satellite can experience a severe malfunction. Satellites with large amounts of software or unhardened COTS electronics would be more vulnerable to such consequential SEUs during the event.

Considering the rate of one SEU per MByte per day in shielded radiation-hardened electronics, we conclude that only a small fraction of conservatively designed satellites would experience severe malfunctions. It is to be noted that SEU rates are strongly device-specific, and the threshold LET and cross-section limits vary by orders of magnitude between devices of different designs and technologies. Hence, our SEU estimates represent specifically a modern radiation hardened satellite data processing component. Satellites with COTS data processing systems with less resilient error correction might experience much higher upset rates, while systems specifically designed for extreme radiation environments might experience lower rates.

We also considered solar cell degradation during the extreme conditions outlined in this paper. The proton EVT spectrum could not be used to estimate solar cell degradation due to it only containing proton energies above $10\,\mathrm{MeV}$ while already protons with only $5\,\mathrm{MeV}$ contribute significantly to solar cell degradation. Hence, we used the CREME96 GEO Peak 5min flux to estimate the solar cell degradation due to Carrington SEP. The solar cell degradation results for GaAs solar cells with more than $200\,\mu\mathrm{m}$ of cover glass also indicate a manageable scenario of less than $2\,\%$ solar cell degradation due to protons and less than $1\,\%$ due to electrons. This would not cause the immediate failure of satellites but would reduce their power budgets, requiring adjustments in operation, especially for satellites that have already used up their degradation margins towards the end of their mission. Like in the case of the TID, this could lead to the early retirement of satellites or reduced service due to changes in satellite operation.

In conclusion, our results largely agree with Odenwald et al. (2006) as our TID, SEU rates and solar cell degradation estimates would not be catastrophic for all satellites but could prematurely retire satellites that were already close to the end of their degradation margins. According to our analysis, satellites may lose up to and over a tenth of their expected mission lifetime from solar cell degradation. The solar cell degradation estimate of Hands et al. (2018) could not be confirmed as, according to our estimate, the degradation is mostly due to SEPs and only on the order of up to $2\,\%$ for typical cover glass thicknesses, while trapped RB electrons cause less than $1\,\%$ solar cell power degradation. Higher cover glass thicknesses would reduce the potential impact of a severe space weather effect, but cover glass alone cannot mitigate the risk entirely. Realistically, missions could consider the financial risk of a significant lifetime loss of solar cells on satellites if a storm of this scale were to occur since we expect reduced solar cell efficiency but not mission loss.

In summary, we conclude that a Carrington-level storm occurring in the near future would not have immediate catastrophic consequences for satellite-based infrastructure. Only a tiny fraction of conservatively designed satellites would show severe

https://doi.org/10.5194/egusphere-2025-1279
Preprint. Discussion started: 26 March 2025

effects. In contrast, "new-space" satellites based on unshielded COTS components and software without adequate error mitigation would experience a higher probability of failure and have their life expectancies significantly reduced. This would result in additional costs and reduced service quality in the "new-space" segment while critical services remain available.

5 Author contribution

The EVT code was written and tested by MS. The EVT analysis, radial diffusion analysis and writing of the EVT sections were completed by MS and AO. AF performed the spectra comparison, TID analysis, and SEE rate estimation and also wrote the corresponding texts. VAK performed the solar cell degradation simulations and wrote the corresponding section. PO acted as project advisor and contributed to the introduction text. MP is the responsible PI for the project, she initialised the work, conceptualised the paper, and contributed to the writing.

6 Funding

This project is one outcome of the Research Council of Finland project CARRINGTON (grant number 339327. MP acknowledges the Research Council of Finland project FAISER (grant number 361901) and the Finnish Centre of Excellence in Research of Sustainable Space (grant number 352846).

Competing interests. One of the (co-)authors, MP, is a member of the editorial board of Annales Geophysicae

Code and data availability. All codes that are required in this paper are described above.

https://doi.org/10.5194/egusphere-2025-1279
Preprint. Discussion started: 26 March 2025

References

Agostinelli, S., Allison, J., Amako, K., Apostolakis, J., Araujo, H., Arce, P., Asai, M., Axen, D., Banerjee, S., Barrand, G., Behner, F., Bellagamba, L., Boudreau, J., Broglia, L., Brunengo, A., Burkhardt, H., Chauvie, S., Chuma, J., Chytracek, R., Cooperman, G., Cosmo, G., Degtyarenko, P., Dell'Acqua, A., Depaola, G., Dietrich, D., Enami, R., Feliciello, A., Ferguson, C., Fesefeldt, H., Folger, G., Foppiano, F., Forti, A., Garelli, S., Giani, S., Giannitrapani, R., Gibin, D., Gómez Cadenas, J., González, I., Gracia Abril, G., Greeniaus, G., Greiner, W., Grichine, V., Grossheim, A., Guatelli, S., Gumplinger, P., Hamatsu, R., Hashimoto, K., Hasui, H., Heikkinen, A., Howard, A., Ivanchenko, V., Johnson, A., Jones, F., Kallenbach, J., Kanaya, N., Kawabata, M., Kawabata, Y., Kawaguti, M., Kelner, S., Kent, P., Kimura, A., Kodama, T., Kokoulin, R., Kossov, M., Kurashige, H., Lamanna, E., Lampén, T., Lara, V., Lefebure, V., Lei, F., Liendl, M., Lockman, W., Longo, F., Magni, S., Maire, M., Medernach, E., Minamimoto, K., Mora de Freitas, P., Morita, Y., Murakami, K., Nagamatu, M., Nartallo, R., Nieminen, P., Nishimura, T., Ohtsubo, K., Okamura, M., O'Neale, S., Oohata, Y., Paech, K., Perl, J., Pfeiffer, A., Pia, M., Ranjard, F., Rybin, A., Sadilov, S., Di Salvo, E., Santin, G., Sasaki, T., Savvas, N., Sawada, Y., Scherer, S., Sei, S., Sirotenko, V., Smith, D., Starkov, N., Stoecker, H., Sulkimo, J., Takahata, M., Tanaka, S., Tcherniaev, E., Safai Tehrani, E., Tropeano, M., Truscott, P., Uno, H., Urban, L., Urban, P., Verderi, M., Walkden, A., Wander, W., Weber, H., Wellisch, J., Wenaus, T., Williams, D., Wright, D., Yamada, T., Yoshida, H., and Zschiesche, D.: Geant4—a simulation toolkit, Nucl. Instrum. Methods Phys. Res. A, 506, 250–303, https://doi.org/10.1016/s0168-9002(03)01368-8, 2003.

Allison, J., Amako, K., Apostolakis, J., Araujo, H., Arce Dubois, P., Asai, M., Barrand, G., Capra, R., Chauvie, S., Chytracek, R., Cirrone, G., Cooperman, G., Cosmo, G., Cuttone, G., Daquino, G., Donszelmann, M., Dressel, M., Folger, G., Foppiano, F., Generowicz, J., Grichine, V., Guatelli, S., Gumplinger, P., Heikkinen, A., Hrivnacova, I., Howard, A., Incerti, S., Ivanchenko, V., Johnson, T., Jones, F., Koi, T., Kokoulin, R., Kossov, M., Kurashige, H., Lara, V., Larsson, S., Lei, F., Link, O., Longo, F., Maire, M., Mantero, A., Mascialino, B., McLaren, I., Mendez Lorenzo, P., Minamimoto, K., Murakami, K., Nieminen, P., Pandola, L., Parlati, S., Peralta, L., Perl, J., Pfeiffer, A., Pia, M., Ribon, A., Rodrigues, P., Russo, G., Sadilov, S., Santin, G., Sasaki, T., Smith, D., Starkov, N., Tanaka, S., Tcherniaev, E., Tome, B., Trindade, A., Truscott, P., Urban, L., Verderi, M., Walkden, A., Wellisch, J., Williams, D., Wright, D., and Yoshida, H.: Geant4 developments and applications, IEEE Trans. Nucl. Sci., 53, 270–278, https://doi.org/10.1109/tns.2006.869826, 2006.

Allison, J., Amako, K., Apostolakis, J., Arce, P., Asai, M., Aso, T., Bagli, E., Bagulya, A., Banerjee, S., Barrand, G., Beck, B., Bogdanov, A., Brandt, D., Brown, J., Burkhardt, H., Canal, P., Cano-Ott, D., Chauvie, S., Cho, K., Cirrone, G., Cooperman, G., Cortés-Giraldo, M., Cosmo, G., Cuttone, G., Depaola, G., Desorgher, L., Dong, X., Dotti, A., Elvira, V., Folger, G., Francis, Z., Galoyan, A., Garnier, L., Gayer, M., Genser, K., Grichine, V., Guatelli, S., Guèye, P., Gumplinger, P., Howard, A., Hřivnáčová, I., Hwang, S., Incerti, S., Ivanchenko, A., Ivanchenko, V., Jones, F., Jun, S., Kaitaniemi, P., Karakatsanis, N., Karamitros, M., Kelsey, M., Kimura, A., Koi, T., Kurashige, H., Lechner, A., Lee, S., Longo, F., Maire, M., Mancusi, D., Mantero, A., Mendoza, E., Morgan, B., Murakami, K., Nikitina, T., Pandola, L., Paprocki, P., Perl, J., Petrović, I., Pia, M., Pokorski, W., Quesada, J., Raine, M., Reis, M., Ribon, A., Ristić Fira, A., Romano, F., Russo, G., Santin, G., Sasaki, T., Sawkey, D., Shin, J., Strakovsky, I., Taborda, A., Tanaka, S., Tomé, B., Toshito, T., Tran, H., Truscott, P., Urban, L., Uzhinsky, V., Verbeke, J., Verderi, M., Wendt, B., Wenzel, H., Wright, D., Wright, D., Yamashita, T., Yarba, J., and Yoshida, H.: Recent developments in Geant4, Nucl. Instrum. Methods Phys. Res. A, 835, 186–225, https://doi.org/10.1016/j.nima.2016.06.125, 2016.

Bagatin, M., Gerardin, S., and Paccagnella, A.: Space and terrestrial radiation effects in flash memories, Semiconductor Science and Technology, 32, 033 003, https://doi.org/10.1088/1361-6641/32/3/033003, 2017.

Baur, C., Gervasi, M., Nieminen, P., Pensotti, S., Rancoita, P. G., and Tacconi, M.: NIEL dose dependence for solar cells irradiated with electrons and protons, in: Astroparticle, Particle, Space Physics and Detectors for Physics Applications - Proceed-

https://doi.org/10.5194/egusphere-2025-1279
Preprint. Discussion started: 26 March 2025

ings of the 14th ICATPP Conference, edited by Giani, S., Leroy, C., Price, L., Rancoita, P.-G., and Ruchti, R., pp. 692–707, https://doi.org/10.1142/9789814603164_0111, provided by the SAO/NASA Astrophysics Data System, 2014.

Binder, D., Smith, E. C., and Holman, A. B.: Satellite Anomalies from Galactic Cosmic Rays, IEEE Transactions on Nuclear Science, 22, 2675–2680, https://doi.org/10.1109/tns.1975.4328188, 1975.

Borowsky, J. E. and Yakymenko, K.: Systems science of the magnetosphere: Creating indices of substorm activity, of the substorm-injected electron population and of the electron radiation belt, J. Geophys. Res. Space Phys., 122, https://doi.org/10.1002/2017ja024250, 2017.

Boteler, D. H.: The super storms of August/September 1859 and their effects on the telegraph system, Advances in Space Research, 38, 159–172, https://doi.org/10.1016/j.asr.2006.01.013, 2006.

Brautigam, D.: CRRES in review: space weather and its effects on technology, Journal of Atmospheric and Solar-Terrestrial Physics, 64, 1709–1721, https://doi.org/10.1016/S1364-6826(02)00121-9, 2002.

Brautigam, D. and Albert, J.: Radial diffusion analysis of outer radiation belt electrons during the October 9, 1990, magnetic storm, J. Geophys. Res. Space Physics, 105, 291–309, https://doi.org/10.1029/1999JA900344, 2000.

Cayton, T. E. and Belian, R. D.: Numerical Modeling of the Synchronous Orbit Particle Analyzer (SOPA, Version 2) that Flew on S/C 1990-095, Los Alamos National Laboratory, 2007.

CERN: GDML Users's Guide: Version 2.8, https://gdml.web.cern.ch/GDML/doc/GDMLmanual.pdf, 2020.

Chapman, S. C., Horne, R. B., and Watkins, N. W.: Using the Index Over the Last 14 Solar Cycles to Characterize Extreme Geomagnetic Activity, Geophysical Research Letters, 47, e2019GL086 524, https://doi.org/10.1029/2019GL086524, 2020.

Chatzikyriakou, E., Morgan, K., and De Groot, C. H. K.: Total Ionizing Dose Hardened and Mitigation Strategies in Deep Submicrometer CMOS and Beyond, IEEE Transactions on Electron Devices, 65, 808–819, https://doi.org/10.1109/ted.2018.2792305, 2018.

Chytracek, R., Mccormick, J., Pokorski, W., and Santin, G.: Geometry Description Markup Language for Physics Simulation and Analysis Applications, IEEE Trans. Nucl. Sci., 53, 2892–2896, https://doi.org/10.1109/tns.2006.881062, 2006.

Cirillo, P. and Taleb, N.: On the statistical properties and tail risk of violent conflicts, Physica A: Statistical Mechanics and its Applications, https://doi.org/10.1016/j.physa.2016.01.050, 2016.

Cirillo, P. and Taleb, N. N.: Tail Risk of Contagious Diseases, Nature Physics, 6, https://doi.org/10.1038/s41567-020-0921-x, 2020.

Coles, S.: An Introduction to Statistical Modeling of Extreme Values, Springer-Verlag London Limited 2001, ISBN 1852334592, 2001.

Doherty, P., Coster, A. J., and Murtagh, W.: Space weather effects of October–November 2003, GPS Solut., 8, 267–271, https://doi.org/10.1007/s10291-004-0109-3, 2004.

Donder, E. D., Messios, N., Calders, S., Calegaro, A., and Mezhoud, S.: SPace ENVironment Information System: SPENVIS, https://www.spenvis.oma.be/, 2018.

Elvidge, S. and Angling, M. J.: Using Extreme Value Theory for Determining the Probability of Carrington-Like Solar Flares, Space Weather, 16, 417–421, https://doi.org/10.1002/2017SW001727, 2017.

Embrechts, P., Klüppelberg, C., and Mikosch, T.: Modelling Extremal Events for Insurance and Finance, Springer, 1997.

ESA: Ionising dose model SHIELDOSE, https://www.spenvis.oma.be/help/background/shieldose/shieldose.html, 2018.

ESA: Space Environment Information System (SPENVIS) Help: Geant4 Radiation Analysis for Space (GRAS), https://www.spenvis.oma.be/help/models/gras%5Fnew.html, accessed: 2024-08-07, 2022a.

ESA: Space Environment Information System (SPENVIS) Help: MC-SCREAM, https://www.spenvis.oma.be/help/models/scream.html, accessed: 2025-01-27, 2022b.

https://doi.org/10.5194/egusphere-2025-1279
Preprint. Discussion started: 26 March 2025

Friedel, R. H. W., Reeves, G. D., and Obara, T.: Relativistic electron dynamics in the inner magnetosphere - a review, Journal of Atmospheric and Solar-Terrestrial Physics, 64, 265–282, https://doi.org/10.1016/s1364-6826(01)00088-8, 2002.

Ginet, G., O'Brien, T., Huston, S., Johnston, W., Guild, T., Friedel, R., Lindstrom, C., Roth, C., Whelan, P., Quinn, R., Madden, D., Morley, S., and Su, Y.-J.: AE9, AP9 and SPM: New models for specifying the trapped energetic particle and space plasma environment, Space Science Reviews, 179, 579–615, https://doi.org/10.1007/s11214-013-9964-y, 2013.

Glauert, S. A., Horne, R. B., and Meredith, N. P.: A 30-year simulation of the outer electron radiation belt, Space Weather, 16, 1498–1522, https://doi.org/10.1029/2018sw001981, provided by the SAO/NASA Astrophysics Data System, 2018.

Hands, A. D. P., Ryden, K. A., Meredith, N. P., Glauert, S. A., and Horne, R. B.: Radiation effects on satellites during extreme space weather events, Space Weather, 16, 1216–1226, https://doi.org/10.1029/2018sw001913, 2018.

Hayakawa, H., Ebihara, Y., Willis, D. M., Toriumi, S., Iju, T., Hattori, K., Wild, M. N., Oliveira, D. M., Ermolli, I., Ribeiro, J. R., Correia, A. P., Ribeiro, A. I., and Knipp, D. J.: Temporal and Spatial Evolutions of a Large Sunspot Group and Great Auroral Storms Around the Carrington Event in 1859, Space Weather, 17, 1553–1569, https://doi.org/10.1029/2019SW002269, 2019.

Heynderickx, D., Quaghebeur, B., Speelman, E., and Daly, E.: ESA's Space Environment Information System (SPENVIS)-A WWW interface to models of the space environment and its effects, in: 38th Aerospace Sciences Meeting and Exhibit, p. 371, https://doi.org/10.2514/6.2000-371, 2000.

Heynderickx, D., Quaghebeur, B., Wera, J., Daly, E. J., and Evans, H. D. R.: New radiation environment and effects models in the European Space Agency's Space Environment Information System (SPENVIS), Space Weather, 2, https://doi.org/10.1029/2004sw000073, 2004.

Heynderickx, D., Quaghebeur, B., Wera, J., Daly, E., and Evans, H.: ESA's SPace ENVironment Information System (SPENVIS): A web-based tool for assessing radiation doses and effects in spacecraft systems, in: Proceedings of the Space Nuclear Conference 2005, pp. 548–552, https://orfeo.belnet.be/handle/internal/4602, 2005.

Horne, R. B., Thorne, R. M., Glauert, S. A., Albert, J. M., Meredith, N. P., and Anderson, R. R.: Timescale for radiation belt electron acceleration by whistler mode chorus waves, J. Geophys. Res. Space Phys., 110, https://doi.org/10.1029/2004JA010811, 2005.

Horne, R. B., Phillips, M. W., Glauert, S. A., Meredith, N. P., Hands, A. D. P., Ryden, K. A., and Li, W.: Realistic Worst Case for a Severe Space Weather Event Driven by a Fast Solar Wind Stream, Space Weather, 16, 1202–1215, https://doi.org/10.1029/2018sw001948, 2018.

Hughes, H. and Benedetto, J.: Radiation effects and hardening of MOS technology: devices and circuits, IEEE Transactions on Nuclear Science, 50, 500–521, https://doi.org/10.1109/tns.2003.812928, 2003.

International Organization for Standardization: ISO 15390:2004, Space environment (natural and artificial) - galactic cosmic ray model, Standard, ISO Geneva, Switzerland, https://www.iso.org/standard/37095.html, 2018.

Jiggens, P., Varotsou, A., Truscott, P., Heynderickx, D., Lei, F., Evans, H., and Daly, E.: The Solar Accumulated and Peak Proton and Heavy Ion Radiation Environment (SAPPHIRE) Model, IEEE Trans. Nucl. Sci., 65, 698–711, https://doi.org/10.1109/tns.2017.2786581, 2018.

Jiggens, P., Clavie, C., Evans, H., O'Brien, T. P., Witasse, O., Mishev, A. L., Nieminen, P., Daly, E., Kalegaev, V., Vlasova, N., Borisov, S., Benck, S., Poivey, C., Cyamukungu, M., Mazur, J., Heynderickx, D., Sandberg, I., Berger, T., Usoskin, I. G., Paassilta, M., Vainio, R., Straube, U., Müller, D., Sánchez-Cano, B., Hassler, D., Praks, J., Niemelä, P., Leppinen, H., Punkkinen, A., Aminalragia-Giamini, S., and Nagatsuma, T.: In Situ Data and Effect Correlation During September 2017 Solar Particle Event, Space Weather, 17, 99–117, https://doi.org/10.1029/2018sw001936, 2019.

Jun, I.: Effects of secondary particles on the total dose and the displacement damage in space proton environments, IEEE Transactions on Nuclear Science, 48, 162–175, https://doi.org/10.1109/23.907581, 2001.

https://doi.org/10.5194/egusphere-2025-1279
Preprint. Discussion started: 26 March 2025

Ketola, V.-A.: Satellite Solar Cell Degradation Estimates for Carrington-Scale Space Weather Events, http://hdl.handle.net/10138/589309, 2024.

Koskinen, H. and Kilpua, E.: Physics of earth's radiation belts: theory and observations, Springer, https://doi.org/10.1007/978-3-030-82167-8, 2022.

Kruglanski, M., Messios, N., De Donder, E., Gamby, E., Calders, S., Hetey, L., Evans, H., and Daly, E.: Last upgrades and development of the space environment information system (SPENVIS), in: 2009 European Conference on Radiation and Its Effects on Components and Systems, pp. 563–565, https://doi.org/10.1109/radecs.2009.5994715, 2009.

LaBel, K. A.: The Space Radiation Environment and Its Effects on Semiconductors and Fiber Optic Systems, in: IEEE International Microwave Symposium, Long Beach, California, 2005.

Lei, F., Truscott, P., Dyer, C., Quaghebeur, B., Heynderickx, D., Nieminen, P., Evans, H., and Daly, E.: MULASSIS: a Geant4-Based Multilayered Shielding Simulation Tool, IEEE Transactions on Nuclear Science, 49, 2788–2793, https://doi.org/10.1109/tns.2002.805351, 2002.

Malandraki, O. E. and Crosby, N. B., eds.: Solar particle radiation storms forecasting and analysis, vol. 444 of *Astrophysics and Space Science Library*, Springer International Publishing, Cham, ISBN 978-3-319-60050-5 978-3-319-60051-2, https://doi.org/10.1007/978-3-319-60051-2, 2018.

Maurer, R. H., Goldsten, J. O., Butler, M. H., and Fretz, K.: Five-Year Results From the Engineering Radiation Monitor and Solar Cell Monitor on the VanAllen Probes Mission, Space Weather, 16, 1561–1569, https://doi.org/10.1029/2018SW001910, 2018.

Messenger, S. R., Walters, R. J., Warner, J. H., Evans, H., Taylor, S. J., Baur, C., and Heynderickx, D.: Status of Implementation of Displacement Damage Dose Method for Space Solar Cell Degradation Analyses, in: 8th European Space Power Conference, vol. 661, p. 98, https://ui.adsabs.harvard.edu/abs/2008ESASP.661E..98M, 2008.

NanoXplore: NG-MEDIUM Radiative Test – Weibull fitting, https://nanoxplore-wiki.atlassian.net/wiki/spaces/NAN/pages/46497810/NG-MEDIUM+Radiative+Test#Weibull-fitting, 2020.

NanoXplore: Announcing the First Space-Qualified European FPGA: NG-Medium, https://nanoxplore.org/index.php/2022/10/16/announcing-the-first-space-qualified-european-fpga-ng-medium/, accessed: 10 March 2025, 2022.

NASA: Spacecraft solar cell arrays, NASA Space Vehicle Design Criteria (Guidance and Control), 1971.

NOAA: Space Weather | National Centers for Environmental Information, https://www.ngdc.noaa.gov/stp/spaceweather.html, accessed: 2024-05-18, 2024.

Normand, E.: Single-event effects in avionics, IEEE Transactions on Nuclear Science, 43, 461–474, https://doi.org/10.1109/23.490893, 1996.

Odenwald, S., Green, J., and Taylor, W.: Forecasting the impact of an 1859-calibre superstorm on satellite resources, Adv. Space Res., 38, 280–297, https://doi.org/10.1016/j.asr.2005.10.046, 2006.

Olla, P., ed.: Space Technologies for the Benefit of Human Society and Earth, Springer Netherlands, Dordrecht, ISBN 978-1-4020-9572-6 978-1-4020-9573-3, https://doi.org/10.1007/978-1-4020-9573-3, 2009.

Osmane, A., Kilpua, E., George, H., Allanson, O., and Kalliokoski, M.: Radial Transport in the Earth's Radiation Belts: Linear, Quasi-linear, and Higher-order Processes, The Astrophysical Journal Supplement Series, 269, 44, https://doi.org/10.3847/1538-4365/acff6a, 2023.

Pickands, J.: Statistical Inference Using Extreme Order Statistics, The Annals of Statistics, 3, https://doi.org/10.1214/aos/1176343003, 1975.

Rathod, S. S., Saxena, A. K., and Dasgupta, S.: Radiation Effects in MOS-based Devices and Circuits: A Review, Iete Technical Review, 28, 451–469, https://doi.org/10.4103/0256-4602.90747, 2011.

https://doi.org/10.5194/egusphere-2025-1279
Preprint. Discussion started: 26 March 2025

Raukunen, O., Usoskin, I., Koldobskiy, S., Kovaltsov, G., and Vainio, R.: Annual integral solar proton fluences for 1984-2019, A&a, 665, A65, https://doi.org/10.1051/0004-6361/202243736, 2022.

Reeves, G. D., Morley, S. K., Friedel, R. H., Henderson, M. G., Cayton, T. E., Cunningham, G., Blake, J. B., Christensen, R. A., and Thomsen, D.: On the relationship between relativistic electron flux and solar wind velocity: Paulikas and Blake revisited, J. Geophys. Res. Space Phys., 116, https://doi.org/10.1029/2010JA015735, 2011.

Rodger, C. J., Verronen, P. T., Clilverd, M. A., Seppälä, A., and Turunen, E.: Atmospheric impact of the Carrington event solar protons, Journal of Geophysical Research Atmospheres, 113, https://doi.org/10.1029/2008JD010702, 2008.

Santin, G., Ivanchenko, V., Evans, H., Nieminen, P., and Daly, E.: GRAS: a general-purpose 3-D Modular Simulation tool for space environment effects analysis, IEEE Trans. Nucl. Sci., 52, 2294–2299, https://doi.org/10.1109/tns.2005.860749, 2005.

Sarma, R., Chandorkar, M., Zhelavskaya, I., Shprits, Y., Drozdov, A., and Camporeale, E.: Bayesian Inference of Quasi-Linear Radial Diffusion Parameters using Van Allen Probes, J. Geophys. Res. Space Phys., 125, e2019JA027 618, https://doi.org/10.1029/2019JA027618, 2020.

Savola, M., Osmane, A., Turc, L., Kilpua, E., Kaheman, K., and Palmroth, M.: Statistical, theoretical and machine learning approaches to estimating maximum electron fluxes, To be submitted, 2025.

Schwenn, R., dal Lago, A., Huttunen, E., and Gonzalez, W. D.: The association of coronal mass ejections with their effects near the Earth, Ann. Geophys., 23, 1033–1059, https://doi.org/10.5194/angeo-23-1033-2005, 2005.

Seltzer, S. M.: SHIELDOSE: a computer code for space-shielding radiation dose calculations, Department of Commerce, National Bureau of Standards, https://doi.org/10.6028/nbs.tn.1116, nBS Technical Note 1116, 1980.

Seltzer, S. M.: Updated calculations for routine space-shielding radiation dose estimates: SHIELDOSE-2, Technical report, US Department of Commerce, National Institute of Standards and Technology, ISSN 199508, https://ntrl.ntis.gov/NTRL/dashboard/searchResults/titleDetail/PB95171039.xhtml, 1994.

Simms, L. E., Pilipenko, V., Engebretson, M. J., Reeves, G. D., Smith, A. J., and Clilverd, M.: Prediction of relativistic electron flux at geostationary orbit following storms: Multiple regression analysis, J. Geophys. Res. Space Physics, 119, 7297–7318, https://doi.org/10.1002/2014JA019955, 2014.

Singleterry, R. C., Blattnig, S. R., Clowdsley, M. S., Qualls, G. D., Sandridge, C. A., Simonsen, L. C., Slaba, T. C., Walker, S. A., Badavi, F. F., Spangler, J. L., Aumann, A. R., Neal Zapp, E., Rutledge, R. D., Lee, K. T., Norman, R. B., and Norbury, J. W.: OLTARIS: On-line tool for the assessment of radiation in space, Acta Astronautica, 68, 1086–1097, https://doi.org/10.1016/j.actaastro.2010.09.022, 2011.

Spjeldvik, W. N.: Transient effects of solar energetic particle flux enhancements on the inner magnetosphere of the Earth, Adv. Space Res., 25, 2307–2310, https://doi.org/10.1016/s0273-1177(99)00513-x, 2000.

Tali, M., Alia, R. G., Brugger, M., Ferlet-Cavrois, V., Corsini, R., Farabolini, W., Javanainen, A., Santin, G., Boatella Polo, C., and Virtanen, A.: Mechanisms of Electron-Induced Single-Event Latchup, IEEE Trans. Nucl. Sci., 66, 437–443, https://doi.org/10.1109/tns.2018.2884537, 2019.

Townsend, L., Zapp, E., Stephens, D., and Hoff, J.: Carrington flare of 1859 as a prototypical worst-case solar energetic particle event, IEEE Trans. Nucl. Sci., 50, 2307–2309, https://doi.org/10.1109/tns.2003.821602, 2003.

Tsurutani, B. T. and Lakhina, G. S.: An extreme coronal mass ejection and consequences for the magnetosphere and Earth, Geophysical Research Letters, 41, 287–292, https://doi.org/10.1002/2013gl058825, 2014.

https://doi.org/10.5194/egusphere-2025-1279
Preprint. Discussion started: 26 March 2025

Tylka, A., Adams, J., Boberg, P., Brownstein, B., Dietrich, W., Flueckiger, E., Petersen, E., Shea, M., Smart, D., and Smith, E.: CREME96: A Revision of the Cosmic Ray Effects on Micro-Electronics Code, IEEE Trans. Nucl. Sci., 44, 2150–2160, https://doi.org/10.1109/23.659030, 1997.

Vainio, R., Desorgher, L., Heynderickx, D., Storini, M., Flückiger, E., Horne, R. B., Kovaltsov, G. A., Kudela, K., Laurenza, M., McKenna-Lawlor, S., Rothkaehl, H., and Usoskin, I. G.: Dynamics of the earth's particle radiation environment, Space Science Reviews, 147, 187–231, https://doi.org/10.1007/s11214-009-9496-7, 2009.

Valtonen, E.: Space Weather Effects on Technology, pp. 241–273, Springer Berlin Heidelberg, Berlin, Heidelberg, ISBN 978-3-540-31534-6, https://doi.org/10.1007/978-3-540-31534-6_8, 2005.